RSC Advances

ROYAL SOCIETY OF CHEMISTRY

www.rsc.org/advances

Magnetic field assisted growth of highly dense α-Fe_2O_3 single crystal nanosheets and their application in water treatment

Dong Lin[a,b], Biwei Deng[a,b], Stephen A. Sassman[c], Yaowu Hu[a,b], Sergey Suslov[b,d], Gary J. Cheng[a,b,e]

[a] *School of Industrial Engineering, Purdue University, West Lafayette, IN, 47906, USA*

[b] *Birck Nanotechnology Center, Purdue University, West Lafayette, IN, 47906, USA*

[c] *Department of Agronomy, Purdue University, West Lafayette, IN, 47906, USA*

[d] *School of Materials Engineering, Purdue University, West Lafayette, IN, 47906, USA*

[e] *School of Mechanical Engineering, Purdue University, West Lafayette, IN, 47906, USA*

Abstract

High dense 2D nanostructures are desirable in photocatalyst, water treatment and energy storage, due to their high surface to volume areas. This paper describes a novel approach combining thermal stress and magnetic force to generate highly dense α-Fe_2O_3 nanosheets on the surface of various iron substrates, including plates and powders. This technique involves the thermal oxidation of iron substrates on the hot plate with magnetic field. The Lorentz force acting on the ions induced by magnetic field facilitates the lateral growth of nanosheet. This effect results in a highly porous nanostructure consisting of dense 2D nanosheets with extremely large BET surface area. The application of these nanosheets is explored in water treatment. Electron microscopic studies indicate that these nanosheets show a parabolic relation with time of thermal oxidation for the growth at width direction. A comparison of heavy metal (As, Cr)[1] ion adsorption of nanosheets and nanowires was also investigated, which shows that nanosheets have a much better adsorption rate than nanowires.

Keywords: Iron, Nanosheet, Thermal oxidation, Magnetic field, Water treatment.

Hematite (α-Fe_2O_3), n-type semiconductor with a small band gap of 2.1 eV[2], has been extensively studied due to the advantage of high theoretical capacity (1007 mAh g^{-1}), environmentally friendliness, nontoxic (in bulk form), corrosion-resistance and low cost[3, 4]. It has been widely applied in the production of gas sensors[4], photocatalysts[5], water treatment[6], magnetic coating for data storage devices[7] and lithium-ion batteries[4]. Stimulated by the promising application of α-Fe_2O_3 and the novel properties of nanoscale materials[2, 4, 8-14], varies methods such as electrodeposition[15], hydrothermal synthesis[16], sol-gel-mediated reactions[6], solvothermal synthesis[17], direct thermal oxidation[2, 6, 18], chemical vapor deposition (CVD)[19], plasma oxidation[20] and plasma-enhanced chemical vapor deposition (PECVD)[21] have been developed to fabricate iron oxide nanostructures. In all of these methods, thermal oxidation of metals holds the advantage for commercial application since it is one of the simplest and most scalable approaches[20, 22]. Large scale of nanowires[7, 22], nanoflakes[23], nanorod[6] were synthesized by thermal oxidation in different circumstances. The nanowires has been generated by thermal oxidation of pure iron in ambient conditions[24]. However, these nanostructures have relatively low area to volume ratio due to the lack of controlled growth in lateral direction. Herein, we report the synthesis of α-Fe_2O_3 nanosheets by thermal oxidation under magnetic field. With applied magnetic field, nanosheets other than nanowires are formed on the iron plate or powder surface. These highly dense nanosheets arrays will be applied to water treatment to test their functionality to reduce heavy metal ions from water.

During the thermal oxidation under magnetic field, the commercial iron plates and powders were heated in the ambient air. The size of iron plates was cut by 1cm × 1 cm. These samples were mechanical polished by 0.05-μm-grade aluminum oxide powder [25-28]. Two different sizes, micron-sized (average size from 4 to 6μm) and nano-sized (from 20 to 100 nm), of iron particles were used. The hot plate with

magnetic stir function was used as heat source. The magnetic force, which acted on iron ions by magnetic field of hot plate (Max magnetic field: 60mT), was applied on iron powders and plate during heating. The temperature of the hot plate was set to 500ºC to study the effect of time and magnetic field on nanosheets generation. In order to study the magnetic field effects, the width of nanosheets was measured by time evolution. Iron plates and powders were also heated to 500ºC in the ambient air without magnetic field to compare with the nanostructures generated with magnetic field.

The mechanism of nanosheet formation is schematically shown in Figure 1. During thermal oxidation, different oxidation layers – FeO, Fe_3O_4 and Fe_2O_3 from bottom to top– were generated subsequently on iron plate. Compressive thermal stress, which is accumulated by the atomic volume difference between Fe_3O_4 and Fe_2O_3 layer, is considered to be the driving force for generating iron oxide nanostructures[2]. Iron ions were driven to the sample surface through grain boundaries in Fe_2O_3 oxidation layer and then move up to the iron oxide nanostructures. As shown in Figure 1(a), the magnetic field is perpendicular to the ion movement direction, which generates Lorentz force on the iron ions. The Lorentz force is on the nuclei plate and also perpendicular to the ion movement driven by thermal stress. As time increase, nanostructures grow on both directions resulting the generation of iron oxide nanosheet.

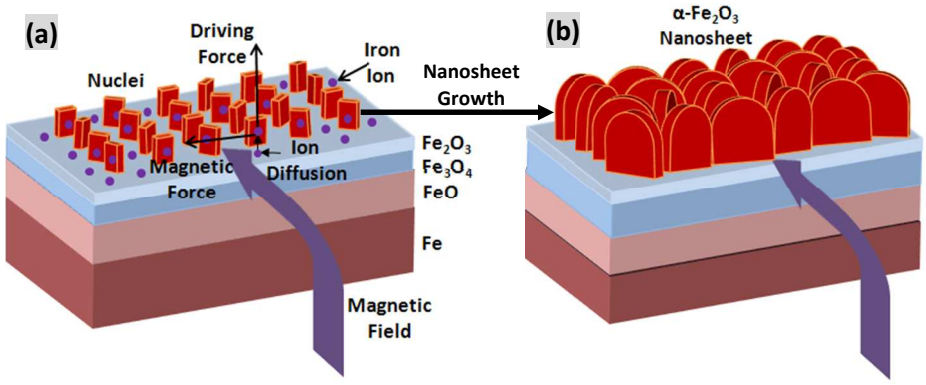

Figure 1. Schematic illustration of α-Fe_2O_3 nanosheet growth under magnetic field: (a) initiation of nanosheet, and (b) growth of nanosheet after several hours.

Figure 2(a) shows large scale and high density of nanosheet growth on the iron plate due to the magnetic field. High density of iron oxide nanosheets were generated by controlling experimental conditions. The iron plate was placed on the middle of the hot plate. It was heated at 500ºC in the ambient air for 14 hours. The nanosheets show a triangular shape, which is wider at the bottom part. The wider bottom parts of nanosheet are affected by Lorentz force. These nanosheets are wider than iron oxide nanowires generated by thermal oxidation method[2, 3, 24]. The α-Fe_2O_3 nanosheets and topmost two oxide layers are shown in Figure 2(b). The Fe_2O_3 and Fe_3O_4 layers can be distinguished by discontinuities in grain size and confirmed by EDS study through investigating oxide and iron atomic ratio. The grain size in Fe_3O_4 layer is flat and large, compared with Fe_2O_3 layer. Based on the study of Sheikh-Ali et al [29], the grain boundary orientation also migrated by annealing in magnetic field. The grain boundaries were reoriented to parallel to samples surface. Dmitri et al.[30] investigated the grain size enlarged by annealing Titanium under magnetic field. After annealing at 1023 K for 240 min under 17T of magnetic field, the mean grain size increased to 139 μm from 39 μm. These two phenomena are both helpful for accumulating thermal stress.

The nanosheet after the processing and its cross section are studied by TEM in Figure 2(c) and (d), respectively. The diffraction pattern (insert of Figure 2(c)) shows that the nanosheet is single crystal, which agrees with former iron oxide nanostructures grown by thermal oxidation method. The thickness of nanosheet in Figure 2(d) is less than 20 nm. The Raman spectrum of nanosheets after thermal oxidation is shown in Figure 2(f). The strong resonant Raman peaks (at 227, 245, 293, 411, 496, 613, 1318 cm^{-1}) in the range of 150-1500 cm^{-1} are in good agreement of α-Fe_2O_3 ($a = 5.038Å, c = 13.772Å$)[31]. Downshift of the resonant peaks was observed from resonant peaks and it may be due to quantum size effect [2]. A weak peak of Fe_3O_4 at 661 cm^{-1} was also sometimes detected in the surface, which is agree with the former results[24]. This signal may come from the oxide layer of sample surface.

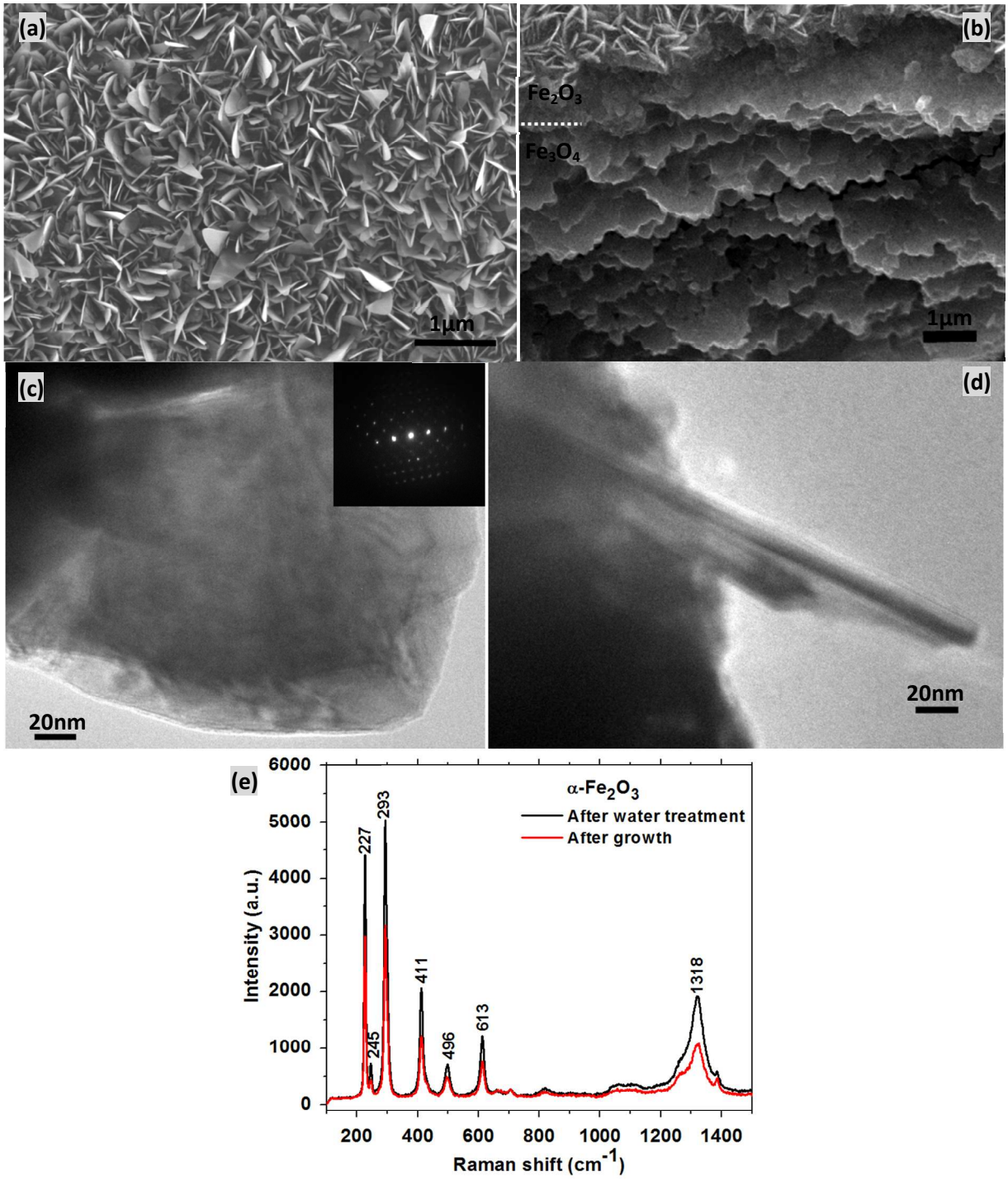

Figure 2. Nanosheet generation at 500ºC in air for 14 hours under magnetic field, (a) surface morphology and (b) cross sectional view of oxidized layers, (c) TEM image of nanosheet, (d) side view of nanosheet, and (e) Raman spectrum of nanosheets before and after water treatment.

The growth of α-Fe_2O_3 nanosheets under magnetic field was further investigated by heating for different time at 500ºC. For α-Fe_2O_3 nanowire generated by thermal oxidation, the growth of α-Fe_2O_3 nanowire is via diffusion of iron ions from iron oxide layers through stacking fault defects in 〈110〉 direction[22, 24]. The Fe_2O_3 oxide layer is topmost and Fe_3O_4, FeO layers are formed subsequently when heating at elevated temperature[24]. They served as the reactants for the inter ion diffusion at high temperature[19]. Compressive force accumulated during heating was considered to be the driving force for the iron ion outward to form nanowire[2]. Enough time and temperature are needed to accumulate compressive thermal stresses. The temperature range for generating iron oxide nanowires is between 300ºC and 900ºC[3]. It needs to be above 300ºC since the rate of stress generation by solid-state phase transformation should sufficient to activate grain boundary diffusion for oxide nanowire growth[2]. When above 900ºC[7], lattice diffusion becomes more favorable than grain boundary diffusion. The time evolution of nanosheet growth under magnetic field is shown in Figure 3[32] for 2, 6, 14 and 24 hours, respectively. Figure 3a shows the initial growth morphology of α-Fe_2O_3 nanosheets. Maximum density of nanosheets was formed on substrate surface after 6 hours of heating. The nanosheet density does not increase after 6 hours. These nanosheets only grow along width and thickness directions.

Yuan et al.[33] found the oxide layer growth following the parabolic growth law, i.e., $x = (2kt)^{1/2}$, where x is the thickness of the oxide layer, k is rate constant, and t is the oxidation time. The widths of nanosheets at different heating times were measured by ImageJ in order to study the magnetic effect. As revealed in Figure 3(e), the mean size of bottom width of nanosheets also follows the parabolic growth law. The growth at the width side proves the effect of magnetic force on nanosheet generation.

The X-ray diffraction (XRD) patterns of as-prepared samples are shown in Figure 3(f). In the XRD pattern of nanosheets, the relative strong Fe_2O_3 peak intensities of the diffraction plane (110) and (214) are much higher than other peaks. While 〈110〉 is the direction of growth direction of nanowires for thermal oxidation method, which gives rise to a relatively intense diffraction peak of the (110) plane[31].The rising of (214) peak may be caused by the magnetic field effects.

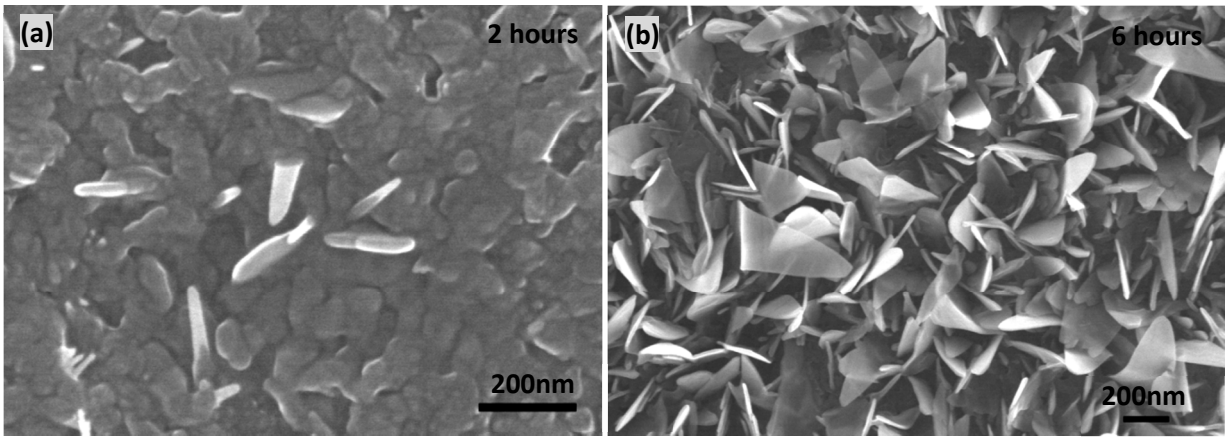

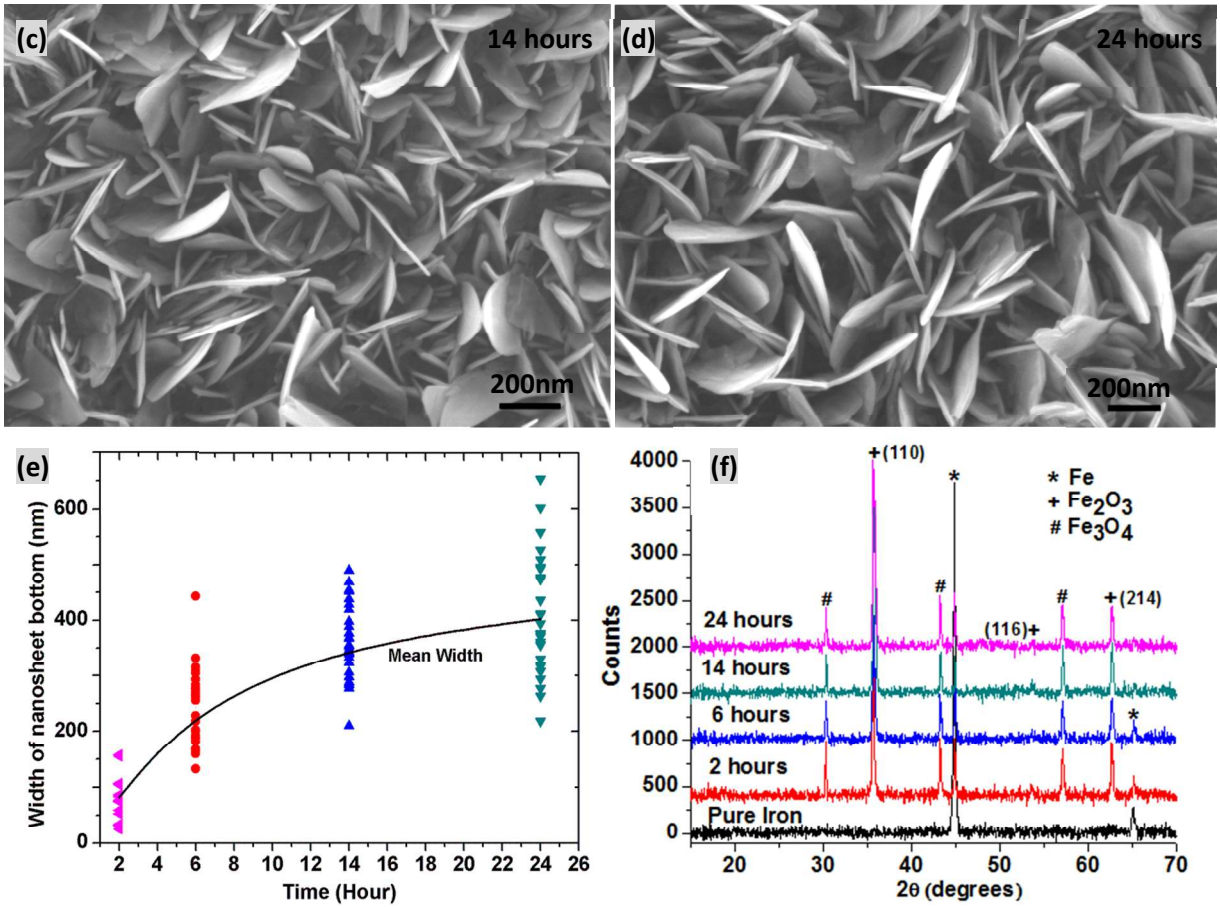

Figure 3. SEM images of iron oxide nanosheet growth of time evolution: (a) 2 hours, (b) 6 hour, (c) 14 hours and (d) 24 hours, at 500ºC under magnetic field, (e) growth in width of nanosheet as function of time (f) XRD patterns of these samples.

The high-density nanosheets can be also grown on micro-sized powders through magnetic assisted thermal oxidation process. The α-Fe_2O_3 nanowires have been grown on micro-sized iron powders [2]. In this study, nanosheets were generated under magnetic field at 500ºC for heating 6 hours, as shown in Figure 4(a). As a comparison, nanowires were generated on micro sized iron powders by heating without magnetic field at 500ºC in air for 6 hours, as shown in Figure 4(b). The cross-sectional view of nanosheet and nanowire can be seen from Figure 4(c) and 4(d), respectively. The height of nanowires ranges from 2 to 3μm, which are longer than nanosheet. However, nanosheets are much wider than the

nanowires, which results in a much higher surface area to volume ratio. The nanosheets are also much a denser than the nanowires. The BET surface area [m^2g^{-1}] value of nanowire and nanosheet on iron powders was measured 16.484 and 70.866, respectively. It shows that surface area of nanosheet is around 4.3 times of nanowire nanostructures, which is a great increase on surface area.

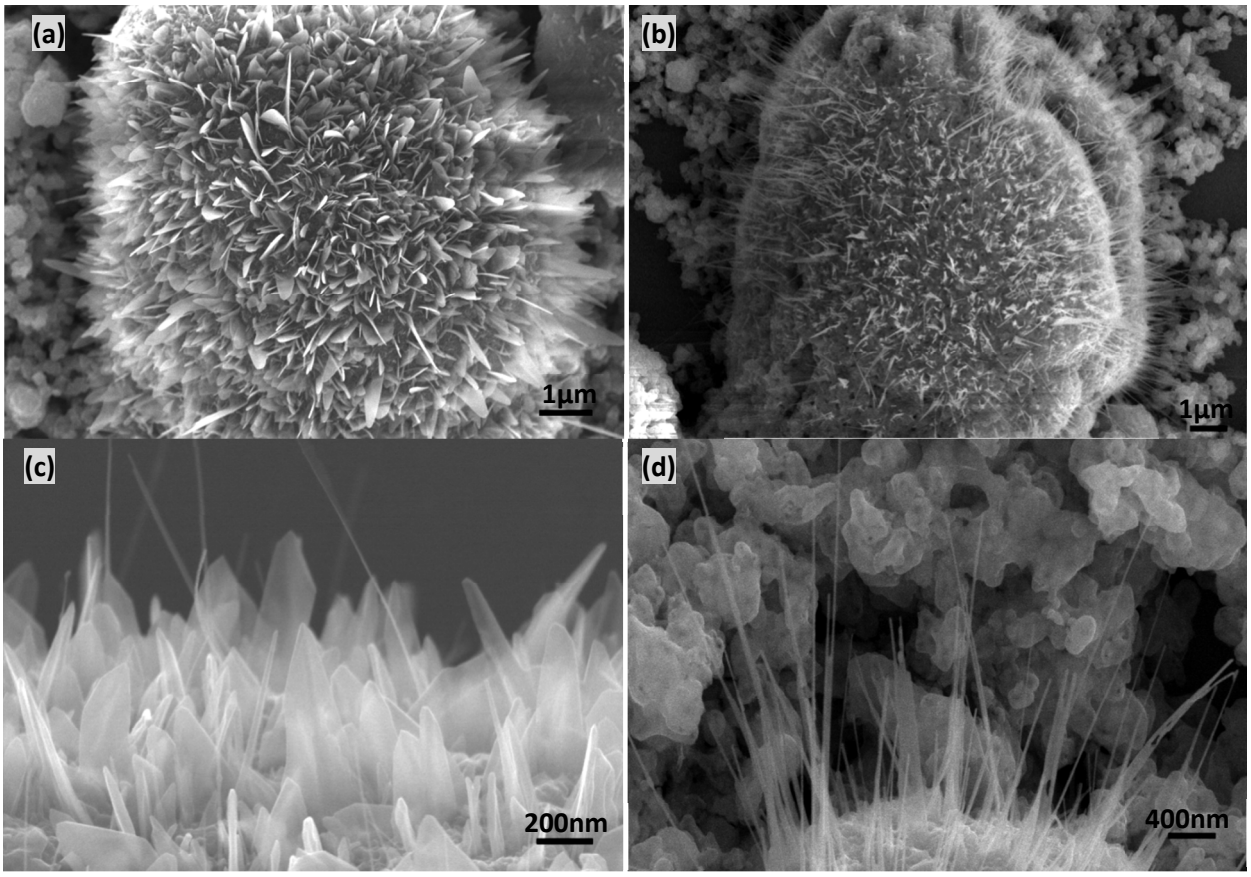

Figure 4. (a) nanosheet generation in air for 6 hours and (b) nanowire generation in air for 6 hours under magnetic field, (c) and (d) vertical view of (a) and (b).

Water pollution is one of the major health and environmental challenge for human society [6, 34]. Removal of heavy metal ions from waste water is an extensive industrial consideration. Currently, the development of using nanomaterials to removal toxic ions from water has attracted much attention. For example, semiconductor nanostructured materials including ZnS, Fe_2O_3, TiO_2 and Cu_2O, have been applied studied

for water treatment[6, 34]. Iron oxide nanomaterials have been used to remove toxic ions from waste water. These materials show high capacities than bulk materials because of their high surface area ratio [6]. Between all the iron oxide materials, the test results show that α-Fe_2O_3 has a better adsorption ability than γ-Fe_2O_3 and Fe_3O_4 [6]. However, mass production of nanomaterials with high surface to volume ratio was still a challenge. Thermal oxidation under magnetic field demonstrates its potential for the practical application of water treatment.

Herein, the powders, with iron oxide nanosheet and nanowires respectively, were synthesized for the application of water treatment. Chromium and arsenic are major highly toxic metal ion in waste water and it is of great importance to remove them from water [6]. Figure 5(a) shows the arsenic concentration variation in 10mL solution as adsorption time increase. Three kinds of iron oxide powders (0.05g) were added in the solution with arsenic concentration of 10 mg/L and the solution was adjusted to pH 4 at room temperature (20ºC). Nanowire, which was grown by thermal oxidation of 24 hours, shows a max of 10% arsenic adsorption. The arsenic adsorption of nanosheet, generated by thermal oxidation under magnetic field of 6 hours, also shows 10% of adsorption after 1 hour water treatment. As a comparison, arsenic can be removed almost 100% after 10 minutes when nanosheets after thermal oxidation for 24 hours were used. For Chromium [1] adsorption in Figure 5(b), 0.05g of nanomaterials, synthesized by thermal oxidation with and without magnetic field respectively, were used for adsorption. 10mL solution with Cr concentration of 10mg/L was prepared and the pH value was adjusted to 3. The adsorption of Cr for nanowire (after 24 hour thermal oxidation) is around 25% percentage after 10 mins, while the adsorption of Cr for nanosheet by thermal oxidation of 6 hours and 24 hours are 50% and 100% after 10 mins, respectively. The nanosheet grown after 24 hours by thermal oxidation under magnetic field shows a better adsorption ratio for both chromium and arsenic ions. These results are consistent with the Figure 3e and 3f, which shows that the width of nanosheet after 24 hours thermal oxidation under magnetic field is maximized. The phase stability of nanosheet was also measured, which is also shown in Figure 2(e). The Raman shifts demonstrate thatα-Fe_2O_3 was stable after water treatment.

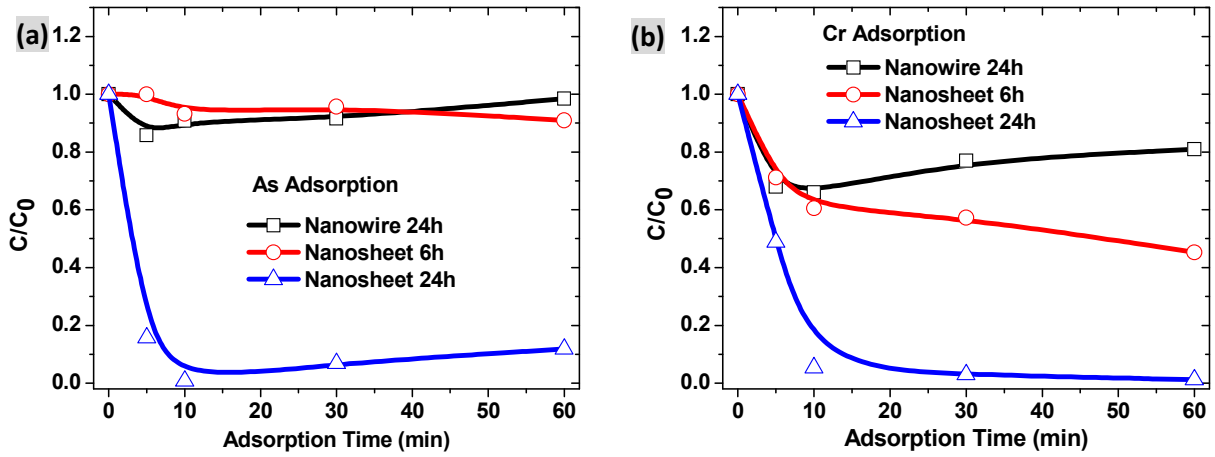

Figure 5. Adsorption rate of (a) As and (b) Cr by various α-Fe_2O_3 nanostructures: nanowire 24 hours, nanosheet 6 hours and nanosheet 24 hours.

It was proposed that the mechanism of removing metal and anionic contaminant is surface complexation and ion exchange between nanostructure surface and heavy metal ions [6]. Higher surface to volume ratio and better nanostructure stability are beneficial for water treatment. Figure 6(a) the morphology of magnetic assisted growth of nanosheet after water treatment for 1 hour. It can be seen that the highly dense nanosheet provide extremely large surface per volume geometry for adsorption of Chromium and Arsenic on to the nanosheet. As a comparison, Figure 6(b) shows the morphology of nanowires grown without magnetic field assisting, after water treatment for 1 hour. The adsorption of Chromium and Arsenic on the nanostructures cannot be observed due to both low surface to volume ratio, and not enough mechanical strength during water treatment. The nanowires are broken from the bottom and washed away, while nanosheets still remains their positions. This is because the nanosheets after thermal oxidization is much more mechanically stable due to the lateral growth under magnetic field. This partially contributes to their much higher absorption of heavy metals.

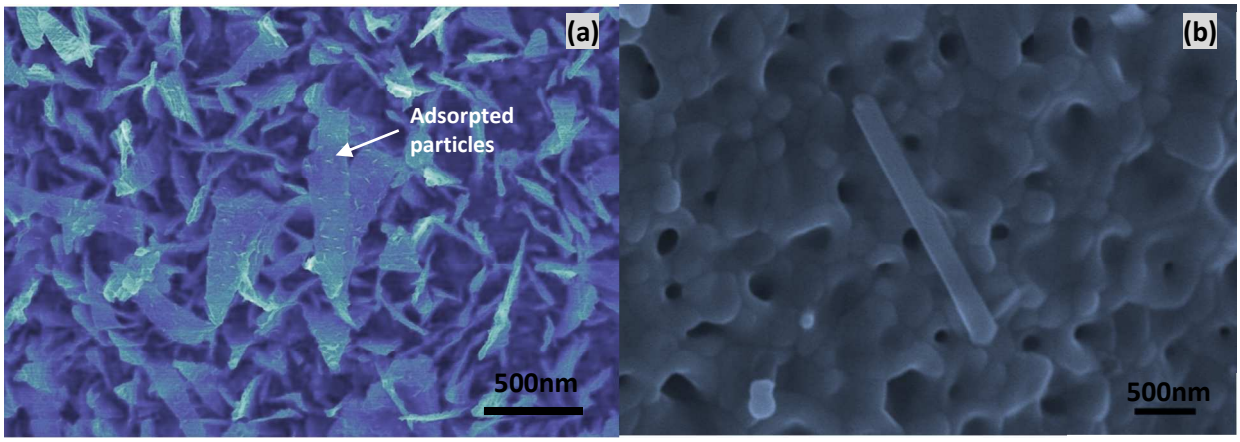

Figure 6. Surface morphology of (a) magnetic assisted growth of nanosheet and (b) nanowire growth without magnetic field assisting after 1 hour water treatment.

In summary, we have demonstrated a procedure combining both thermal oxidation and magnetic field to generate high density and large scale of α-Fe_2O_3 nanosheet on both iron plate and powders. Both Raman and XRD studies indicated that these nanosheets are α-Fe_2O_3 nanostructures. The evolution of shape of the nanosheets and grain distribution in the cross section were studied to reveal the effect of magnetic field for the synthesis of α-Fe_2O_3 nanosheet. Nanosheets (70.866) have much higher BET surface area than nanowires (16.484) and are also more stable during water treatment. These results in excellent adsorption of heavy metal ion in water treatment.

Reference

1. J. S. Bunch, S. S. Verbridge, J. S. Alden, A. M. van der Zande, J. M. Parpia, H. G. Craighead and P. L. McEuen, *Nano Letters*, 2008, 8, 2458-2462.
2. Y. Y. Fu, R. M. Wang, J. Xu, J. Chen, Y. Yan, A. V. Narlikar and H. Zhang, *Chemical Physics Letters*, 2003, 379, 373-379.
3. P. Hiralal, H. E. Unalan, K. G. U. Wijayantha, A. Kursumovic, D. Jefferson, J. L. MacManus-Driscoll and G. A. J. Amaratunga, *Nanotechnology*, 2008, 19, 455608.
4. J. Chen, L. Xu, W. Li and X. Gou, *Advanced Materials*, 2005, 17, 582-586.

5. J. S. Jang, H. G. Kim, V. R. Reddy, S. W. Bae, S. M. Ji and J. S. Lee, *Journal of Catalysis*, 2005, 231, 213-222.
6. L. S. Zhong, J. S. Hu, H. P. Liang, A. M. Cao, W. G. Song and L. J. Wan, *Advanced Materials*, 2006, 18, 2426-2431.
7. T. Tepper, F. Ilievski, C. A. Ross, T. R. Zaman, R. J. Ram, S. Y. Sung and B. J. H. Stadler, *Journal of Applied Physics*, 2003, 93, 6948-6950.
8. S. F. Hasany, N. H. Abdurahman, A. R. Sunarti and R. Jose, *Current Nanoscience*, 2013, 9, 561-575.
9. M. L. Kahn, A. Glaria, C. Pages, M. Monge, L. Saint Macary, A. Maisonnat and B. Chaudret, *Journal of Materials Chemistry*, 2009, 19, 4044-4060.
10. M. I. Dar and S. Shivashankar, *RSC Advances*, 2014, 4, 4105-4113.
11. L. Yuan, R. Cai, J. I. Jang, W. Zhu, C. Wang, Y. Wang and G. Zhou, *Nanoscale*, 2013, 5, 7581-7588.
12. L. Yuan, Q. Jiang, J. Wang and G. Zhou, *Journal of Materials Research*, 2012, 27, 1014-1021.
13. L. Yuan, Y. Wang, R. Cai, Q. Jiang, J. Wang, B. Li, A. Sharma and G. Zhou, *Materials Science and Engineering: B*, 2012, 177, 327-336.
14. R. Cai, T. Li, Y. Wang, C. Wang, L. Yuan and G. Zhou, *Journal of Nanoparticle Research*, 2012, 14, 1-11.
15. L. Y. Zhang, D. S. Xue, X. F. Xu, A. B. Gui and C. X. Gao, *Journal of Physics: Condensed Matter*, 2004, 16, 4541.
16. D. Chen and L. Gao, *Chemical Physics Letters*, 2004, 395, 316-320.
17. J. Jin, S. Ohkoshi and K. Hashimoto, *Advanced Materials*, 2004, 16, 48-51.
18. Y. M. Zhao, Y.-H. Li, R. Z. Ma, M. J. Roe, D. G. McCartney and Y. Q. Zhu, *Small*, 2006, 2, 422-427.
19. Y. L. Chueh, M. W. Lai, J. Q. Liang, L. J. Chou and Z. L. Wang, *Advanced Functional Materials*, 2006, 16, 2243-2251.
20. U. Cvelbar, Z. Chen, M. K. Sunkara and M. Mozetič, *Small*, 2008, 4, 1610-1614.
21. F. Liu, P. J. Cao, H. R. Zhang, J. F. Tian, C. W. Xiao, C. M. Shen, J. Q. Li and H. J. Gao, *Advanced Materials*, 2005, 17, 1893-1897.
22. C. J. Love, J. D. Smith, Y. Cui and K. K. Varanasi, *Nanoscale*, 2011.
23. P. M. Rao and X. Zheng, *Nano Letters*, 2009, 9, 3001-3006.
24. A. Nasibulin, S. Rackauskas, H. Jiang, Y. Tian, P. Mudimela, S. Shandakov, L. Nasibulina, S. Jani and E. Kauppinen, *Nano Research*, 2009, 2, 373-379.
25. D. Lin, M. Y. Zhang, C. Ye, Z. Liu, C. R. Liu and G. J. Cheng, *Applied Surface Science*, 2012, 258, 4254-4259.
26. D. Lin, Y. Yang and G. J. Cheng, *Applied Surface Science*, 2013, 283, 924-929.
27. D. Lin, S. Suslov, C. Ye, Y. Liao, C. R. Liu and G. J. Cheng, *Applied Surface Science*, 2011.
28. D. Lin, C. Ye, Y. Liao, S. Suslov, R. Liu and G. J. Cheng, *Journal of Applied Physics*, 2013, 113, 133509.
29. A. D. Sheikh-Ali, D. A. Molodov and H. Garmestani, *Scripta Materialia*, 2003, 48, 483-488.
30. C. B. Dmitri A. Molodov, Peter J. Konijnenberg, Luis A. Barrales-Mora and Volker Mohles, *Materials Transactions*, 2007, 48, 2800-2808.
31. X. Wen, S. Wang, Y. Ding, Z. L. Wang and S. Yang, *The Journal of Physical Chemistry B*, 2004, 109, 215-220.
32. M. Terrones, O. Martín, M. González, J. Pozuelo, B. Serrano, J. C. Cabanelas, S. M. Vega-Díaz and J. Baselga, *Advanced Materials*, 2011, 23, 5302-5310.
33. L. Yuan, Y. Wang, R. Mema and G. Zhou, *Acta Materialia*, 2011, 59, 2491-2500.
34. H. Chen and J. He, *The Journal of Physical Chemistry C*, 2008, 112, 17540-17545.